Composition dependence of the in-plane Cu-O bond-stretching LO phonon mode in $YBa_2Cu_3O_{6+x}$

F. Stercel,[1] T. Egami,[2,3,4] H. A. Mook,[4] M. Yethiraj,[4,5] J.-H. Chung,[1,6] M. Arai,[7] C. Frost,[8] and F. Dogan[9]
[1]*Department of Materials Science and Engineering, University of Pennsylvania, Philadelphia, Pennsylvania 19104, USA*
[2]*Joint Institute for Neutron Sciences, University of Tennessee, Knoxville, Tennessee 37996, USA*
[3]*Department of Materials Science and Engineering and Department of Physics and Astronomy, University of Tennessee, Knoxville, Tennessee 37996, USA*
[4]*Oak Ridge National Laboratory, Oak Ridge, Tennessee 37831, USA*
[5]*Bragg Institute, ANSTO, Menai, New South Wales 2234, Australia*
[6]*Department of Physics, Korea University, Seoul 126-713, Korea*
[7]*J-PARC Centre, Japan Atomic Energy Agency, Tokai 319-1195, Japan*
[8]*Rutherford Appleton Laboratory, Didcot, Oxon OX11 0QX, United Kingdom*
[9]*Department of Materials Science, University of Missouri, Rolla, Missouri 65409, USA*
(Received 25 September 2007; published 4 January 2008)

An inelastic pulsed neutron scattering study was performed on the dependence of the dispersion and spectral intensity of the in-plane Cu-O bond-stretching LO phonon mode on doped charge density. The measurements were made in the time-of-flight mode with the multiangle position sensitive spectrometer of the ISIS facility on single crystals of $YBa_2Cu_3O_{6+x}$ (x=0.15, 0.35, 0.6, 0.7, and 0.95). The focus of the study is the in-plane Cu-O bond-stretching LO phonon mode, which is known for strong electron-phonon coupling and unusual dependence on composition and temperature. It is shown that the dispersions for the samples with x=0.35, 0.6, and 0.7 are similar to the superposition of those for x=0.15 and 0.95 samples, and cannot be explained in terms of the structural anisotropy. It is suggested that the results are consistent with the model of nanoscale electronic phase separation, with the fraction of the phases being dependent on the doped charge density.

DOI: 10.1103/PhysRevB.77.014502 PACS number(s): 74.25.Kc, 63.20.K−, 71.30.+h, 74.20.Mn

I. INTRODUCTION

Phonons in cuprate superconductors have been studied extensively by inelastic neutron scattering, and the phonon dispersion relations were determined for single crystal samples of $La_{2-x}Sr_xCuO_4$ and $YBa_2Cu_3O_{6+x}$.[1] Whereas most of the phonon modes depend only weakly on doping charge density and can be well explained by a model of lattice dynamics with mainly a pairwise interaction,[2] some modes, the in-plane Cu-O bond-stretching longitudinal optical (LO) mode in particular, show unusual dependence on charge density and temperature. For instance, the LO mode at $\boldsymbol{Q}=(\pi,0)$ (in the unit of $1/a$, where a is the in-plane lattice constant), the half-breathing mode, was observed to soften significantly with doping both for $La_{2-x}Sr_xCuO_4$ and $YBa_2Cu_3O_{6+x}$ systems.[1] This softening cannot be accounted for by simple potential models and needs more complex models to explain.[3–5] Temperature variations of this mode in $La_{1.85}Sr_{0.15}CuO_4$ (Refs. 6 and 7) and $YBa_2Cu_3O_{6.95}$ (Refs. 8–10) are also nontrivial and unusual. In addition, certain features of this mode attract attention. For example, the phonon densities of states in $La_{2-x}Sr_xCuO_4$ powder samples with different doping charge densities show that a peak appears at 72 meV, above the concentration of metal-insulator transition ($x\sim0.07$).[11] This peak is the signature of the softened in-plane Cu-O bond-stretching mode at the zone boundary. The peak is not present in any of the insulating $La_{2-x}Sr_xCuO_4$ samples and is present in all superconducting samples. The measurements of phonon dispersion by inelastic x-ray scattering[12] and inelastic neutron scattering,[13] on the other hand, suggest that the energy for the zone-boundary mode becomes constant beyond $x\sim0.12$, in apparent contradiction to the density of state results.

An important reason to focus on this mode is that it is expected to couple strongly to electrons. Since this mode modulates the distance between Cu and O, and thus the overlap between the Cu d orbital and the O p orbital, it induces charge transfer between Cu and O, resulting in strong electron-phonon coupling.[14–16] Indeed, the angle-resolved photoelectron spectroscopy (ARPES) study has identified this mode to be coupling strongly to electrons.[17,18] While phonons are often considered to be harmful to the d-wave superconductivity mediated by spin fluctuations, spin fluctuation has not been positively identified as the sole microscopic mechanism of the cuprate superconductivity, in spite of extensive studies. It is possible that the phonons are involved in the microscopic mechanism in some complex manner,[19] and thus the phonons in the cuprates deserve a careful study.

It should be noted that most of the reports on the Cu-O bond-stretching modes in the $La_{2-x}Sr_xCuO_4$ and $YBa_2Cu_3O_{6+x}$ systems focused on the dispersion alone and not on the spectral intensities. In this work, we present the results of inelastic neutron scattering measurements on five $YBa_2Cu_3O_{6+x}$ single crystals with nominal oxygen content of x=0.15, 0.35, 0.6, 0.7, and 0.95. We put a particular emphasis on both the energy and the spectral intensity of the Cu-O bond-stretching mode near $(\pi,0)$. Lattice dynamical calculations have also been performed to elucidate the experimentally observed phonon behavior.

II. EXPERIMENTAL METHODS AND RESULTS

The neutron inelastic scattering measurements were carried out with the multiangle position sensitive (MAPS)

spectrometer of the ISIS pulsed neutron facility at the Rutherford-Appleton Laboratory in the time-of-flight mode. Single crystal samples of $YBa_2Cu_3O_{6+x}$, each weighing from 25 to 106 g, were used for the measurement. Neutron scattering showed that the samples with $x=0.15$ and 0.35 were tetragonal, while others were orthorhombic at the temperatures of measurement (9 K), and were twinned. The samples were mounted on a specimen holder, with one of the twinned a/b axes and the c axis in the horizontal plane, and the other a/b axis being vertical. The specimen holder was encapsulated in an aluminum can, filled with helium gas, in order to provide a heat-conducting medium between the sample and the closed cycle helium refrigerator (displex). Using the 16 m^2 array of position sensitive detectors, counts were collected in 147 456 pixel elements and 200 energy channels. The incident energy was chosen to be 120 meV. The energy resolution depends on the chopper frequency and the energy transfer. In our case, the resolution was 5 meV for elastic scattering and 3 meV for 60 meV energy transfer. With MAPS, one measures the scattered intensity as a function of two components of the momentum transfer $\boldsymbol{Q}$, and the energy transfer $\hbar\omega$: $I(\boldsymbol{Q},\omega)$. The third component of the momentum transfer is a function of ω and Q_x, Q_y. For simplicity, we are going to use Miller indices to denote the components of $\boldsymbol{Q}$. The crystals were oriented in such a way that L $(Q_z)=0$ at 55 meV. Thus, in our study we primarily focus on the Δ_1 mode.

The phonon dispersion can readily be obtained by identifying peaks in $I(\boldsymbol{Q},\omega)$. However, in this study we focus on the spectral intensity as well. For that reason a much more careful quantitative data reduction was necessary in order to obtain the normalized dynamic structure factor $S(\boldsymbol{Q},\omega)$. First, the momentum-independent background was removed. $I(\boldsymbol{Q},\omega)$ was converted to $I(Q,\omega)$, where $Q=|\boldsymbol{Q}|$. $I(Q,\omega_i)$ was then determined for 10 meV intervals of $\hbar\omega$ around $\hbar\omega_i$ by integrating $I(Q,\omega)$ over the respective intervals. The intensity of each of these "slices" was fitted to

$$I(Q,\omega)=I_o(\omega)+[I_1(\omega)Q^2+I_2(\omega)Q^4]e^{-\langle U\rangle Q^2} \tag{1}$$

to obtain the momentum-independent background, denoted by $I_o(\omega)$, where I_1 and I_2 are the one- and two-phonon intensities, respectively; $\langle U\rangle$ is the unit cell averaged isotropic thermal factor. Scattering intensities resulting from higher-order phonon scattering processes were neglected. Thus, we obtained $I_o(\omega)$ for $\hbar\omega=5,10,\ldots,85$ meV. These values of I_o were fitted to a polynomial. The two-phonon intensity is proportional to the self-convoluted phonon density of states. The experimental phonon density of states is available in literature. The function $I_2(Q,\omega)$ was calculated in the following way: $I_1(Q,\omega)=0$ for $\hbar\omega>\hbar\omega_{\max}=80$ meV (maximum single phonon energy); therefore, $I_2(Q,\omega_{max})=I(Q,\omega_{max})-I_o(\omega_{max})$. Using this,

$$I_2(Q,\omega)=I_2(Q,\omega_{max})\frac{\mathrm{conv}[Z,\omega]}{\mathrm{conv}[Z,\omega_{max}]}Q^4e^{-\langle U\rangle Q^2}, \tag{2}$$

where $Z(\omega)$ is the phonon density of states and $\mathrm{conv}[Z,\omega]$ is a self-convolution of the function $Z(\omega)$,

$$\mathrm{conv}[Z,\omega]=\int_{-\infty}^{\infty}Z(\omega-z)Z(z)dz. \tag{3}$$

Finally, the one-phonon intensity is given by

$$I_1(Q,\omega)=I(Q,\omega)-I_o(\omega)-I_2(Q,\omega). \tag{4}$$

The reduced dynamical structure factor for single-phonon scattering was obtained by correcting for the thermal factors,

$$\mathfrak{I}(Q,\omega)=I_1(Q,\omega)\frac{\hbar\omega}{1-e^{-\hbar\omega/kT}}\frac{1}{Q^2e^{-\langle U\rangle Q^2}}. \tag{5}$$

In this form, intensities can be compared for different energies and Brillouin zones. In addition, to allow the comparison of different samples, the intensities were normalized by the total intensity obtained by integrating the dynamical structure factor over the entire $(\boldsymbol{Q},E)$ space included in Fig. 1. Due to the fixed geometry of the measurement, only two components of $\boldsymbol{Q}$ are independent. Phonon dispersion and its spectral intensity were determined by integrating $\mathfrak{I}(\boldsymbol{Q},\omega)$ over $h\in[h_i-0.05,h_i+0.05]$ and $k\in[-0.1,0.1]$ intervals for $h_i=2.5,2.6,\ldots,3.5$. Hence, we obtained phonon spectral intensities as functions of energy transfer for a series of h values. The reduced dynamical structure factors for all five compositions of $YBa_2Cu_3O_{6+x}$ are shown as two dimensional intensity plots in Fig. 1. A multiple Gaussian peak fit was performed using existing dispersion data and theoretical models as a guide to identify phonon modes,[8,20] as shown in Fig. 2.

Figure 1 shows that the variation in the dispersion with composition is not a smooth evolution, as has been suggested for $La_{2-x}Sr_xCuO_4$.[12,13] Instead, except for the $x=0.15$ sample, the basic outlook of the dispersion is remarkably similar, as pointed out by our preliminary study.[21] The $x=0.15$ sample has a nearly dispersionless mode at 69–73 meV. The $x=0.95$ sample shows a strongly dispersing mode, with a characteristic softening toward the zone edge with the energy falling down from 66–72 meV at the zone center to 55–58 meV at the zone edge. It appears that the dispersions in the samples with intermediate doping ($x=0.35$, 0.6, and 0.7) are made of superposition of the dispersion in the $x=0.15$ sample (high-energy branch) and the dispersion in the $x=0.95$ sample (low-energy branch). Due to orthorhombic distortion, the dispersion is split into two sub-branches for $x>0.35$. For $YBa_2Cu_3O_{6.6}$, it has been argued that these two branches are due to the a-b anisotropy.[9] However, the two branches are similarly present in $YBa_2Cu_3O_{6.35}$, which is tetragonal and therefore without the a-b anisotropy. The effects of the a-b anisotropy are, indeed, present in the orthorhombic compounds, but appear to be most pronounced at the zone center, where the splitting is clearly seen.

As pointed out earlier,[21] the difference between the energy at the zone center and the zone edge, hence the softening of the phonon mode, is approximately the same for $YBa_2Cu_3O_{6.35}$, $YBa_2Cu_3O_{6.6}$, $YBa_2Cu_3O_{6.7}$, and $YBa_2Cu_3O_{6.95}$. Figure 3 shows the fitted peak positions at the zone center and the zone edge. Indeed, the softening is $\sim$14 meV for all compositions, while naively the bond-stretching mode is expected to soften gradually with increas-

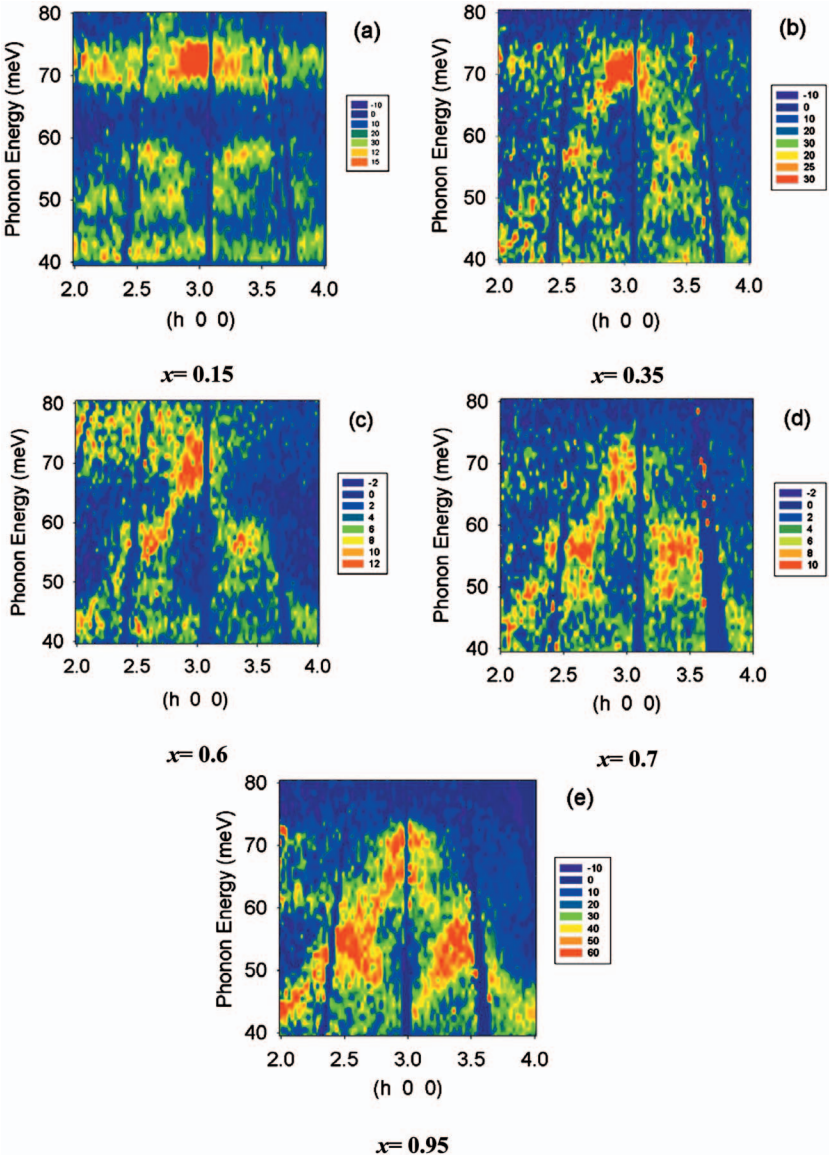

FIG. 1. (Color) The reduced dynamical structure factor of $YBa_2Cu_3O_{6+x}$ at $T=9$ K for various doping levels determined by time-of-flight inelastic neutron scattering by MAPS, in arbitrary units. The actual compositions are (a) $YBa_2Cu_3O_{6.15}$ (insulating), (b) $YBa_2Cu_3O_{6.35}$ (onset of superconductivity), (c) $YBa_2Cu_3O_{6.6}$ (underdoped), (d) $YBa_2Cu_3O_{6.7}$ (underdoped), and (e) $YBa_2Cu_3O_{6.95}$ (optimally doped). Data were integrated from $k=-0.1$ to 0.1. The nearly vertical blue gaps are due to gaps in the position sensitive detector array.

ing hole concentration. In addition, Fig. 1 shows that the intensity of the softened zone-edge mode increases with doping.

The evaluation of the spectral intensity is less straightforward than identifying the dispersion because of the presence of additional modes. First, a nearly dispersionless c axis apical oxygen Raman mode is present in the same energy range.[8,9] In $YBa_2Cu_3O_{6.95}$ as well as in $YBa_2Cu_3O_{6.15}$ this c-axis mode is mostly well separated from the bond-stretching mode; therefore, we can easily evaluate its intensity. Its energy varies slightly with doping, from ~57.5 meV for $x=0.15$ to ~62 meV for $x=0.95$. In $YBa_2Cu_3O_{6.35}$, $YBa_2Cu_3O_{6.6}$, and $YBa_2Cu_3O_{6.7}$, however, this mode mixes with the bond-stretching mode. We assumed that the intensity of the c-axis mode is a linear function of the oxygen content throughout the entire composition range. For $YBa_2Cu_3O_{6.6}$, $YBa_2Cu_3O_{6.7}$, and $YBa_2Cu_3O_{6.95}$, the modes split because of the orthorhombic distortion. In addition to $YBa_2Cu_3O_{6.95}$, the bond-bending mode overlaps with the stretching mode at the zone edge. Again, the intensity of the bond-bending mode at the zone edge was estimated by extrapolation from the portion of the $\boldsymbol{Q}$ space where there is no overlap. After subtracting the intensity of the c-axis mode from that of the bond-stretching mode for $YBa_2Cu_3O_{6.35}$, $YBa_2Cu_3O_{6.6}$, and $YBa_2Cu_3O_{6.7}$ and the intensity of the bond-bending mode from that of the bond-stretching mode for $YBa_2Cu_3O_{6.95}$, the spectral intensity of the high-energy branch and that of the low-energy branch at the zone edge were evaluated, as shown in Fig. 4. The result shows that the intensity of the high-energy branch decreases nearly linearly, while the intensity of the low-energy branch increases also linearly, with increasing doping, indicating the shift in the spectral weight without changing the dispersion.

III. ANALYSIS OF THE RESULTS

In order to investigate the effects of doping on the in-plane Cu-O bond-stretching mode, we carried out shell model calculations. The parameters of the shell model were taken from Ref. 22, but not including the special force constants introduced in that model to stabilize the low-energy

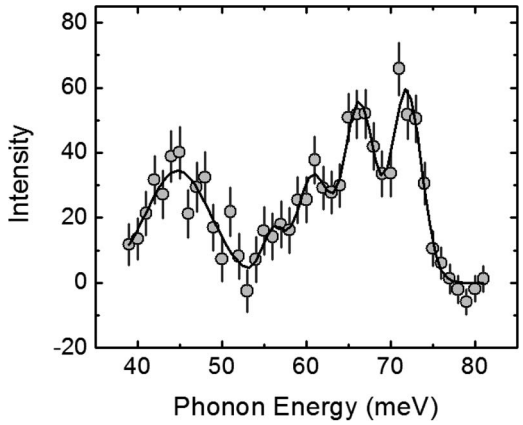

FIG. 2. An example of a constant-$\boldsymbol{Q}$ cut taken at $h=3.0$ and $k=0.0$. Gaussian peak fitting was used to determine the position and intensity of phonon branches.

phonons. As a starting point, we calculated the dispersion and phonon intensities for $YBa_2Cu_3O_{6.95}$ with the nominal charge density as in Ref. 22. We neglected the orthorhombic distortion for the sake of simplicity. In this case, the softening of the bond-stretching mode was not reproduced. Then, the charge density parameter in the shell model was changed according to the doping levels of the other three compounds considered in this work in the following way. In the first model, the charge on the in-plane oxygen shells was changed by $\delta q=-0.1\times(1-x)$, where x is the doped oxygen content in $YBa_2Cu_3O_{6+x}$. To maintain charge neutrality, a charge of $-2\delta q$ was added to the core of the Ba atoms. The model assumes that charge density is homogeneous in the plane. The parameters of the interaction potentials were kept constant. Calculated phonon intensities, convoluted with the instrumental resolution, are shown in Fig. 5. Symbols marked with "Series 1" in Figs. 6 and 7 show the energy and the spectral intensity of the bond-stretching mode at the zone boundary. This model could not account for the softening of

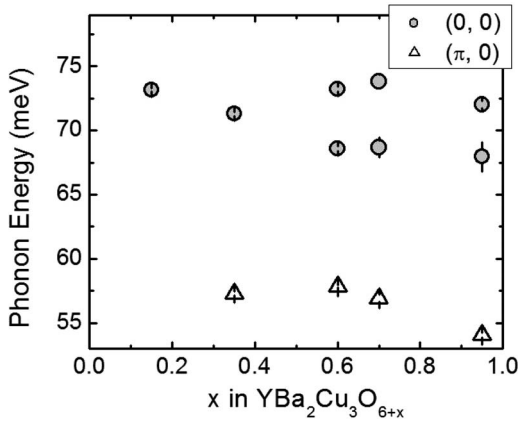

FIG. 3. Energies of the in-plane Cu-O bond-stretching LO mode at the zone center and the zone edge in the four different compounds investigated. The extent of the softening (the difference between the zone-center and zone-edge energies) is essentially the same for all superconducting compounds. There is no softened mode in $YBa_2Cu_3O_{6.15}$.

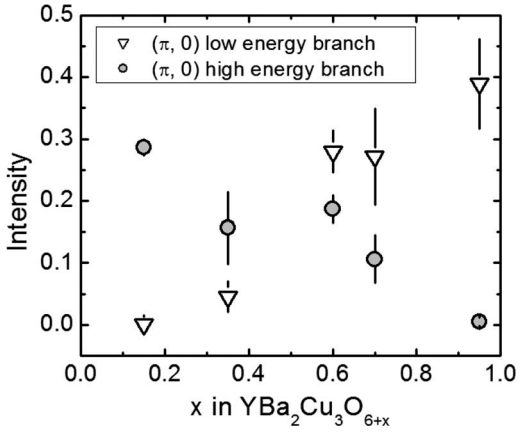

FIG. 4. Intensities of the high-energy branch and the low-energy branch of the in-plane Cu-O bond-stretching LO mode at the zone edge. Since there is no soft mode in $YBa2Cu3O_{6.15}$, the low-energy branch has zero intensity for this compound. Also, there was virtually no intensity to assign to the high-energy branch in $YBa_2Cu_3O_{6.95}$. It is clear that the spectral weight is transferred from the high-energy branch to the low-energy branch with increasing doping, and both branches exist within the same compound of intermediate doping levels.

the bond-stretching mode nor the coexistence of two stretching modes in the $x=0.35$, 0.6, and 0.7 samples.

In the second set of calculations, additional harmonic terms were introduced for O_{plane}-O_{plane}, O_{plane}-O_{apical}, and Cu_{plane}-O_{apical} interaction potentials for in-plane oxygen atoms along the a direction to reproduce the zone-boundary softening of the in-plane Cu-O bond-stretching mode, as in Ref. 6. The potentials were the same for all four compounds, and the charge density was adjusted according to doping levels in each compound. This set of calculations reproduced the softening of the stretching mode, but not the coexistence of two stretching-mode branches (Fig. 8). Also, the intensity of the stretching mode at the zone boundary at 57 meV was nearly constant as a function of doping, contrary to experimental observations (Series 2 in Figs. 6 and 7).

In the third set of simulations, the parameters of the additional harmonic potential were changed so that the coefficients of the potential are proportional to the charge density (Table I) except for the insulator ($x=0.15$), where harmonic potentials were omitted (Fig. 9). The results show that the zone-boundary energy of the stretching mode is not constant, but gradually decreases with increasing doping (Series 3 in Fig. 9). Neither changing the charge density alone nor changing the charge density and the interaction potentials between copper and oxygen atoms could account for the experimentally observed composition dependence of stretching mode phonon energies and intensities.

In order to explain the presence of two greatly different branches in $YBa_2Cu_3O_{6.6}$, Ref. 9 assumed very strong a-b anisotropy involving the mixing with the c-axis apical oxygen mode. The anisotropy in dispersion for $YBa_2Cu_3O_{6.95}$ due to the orthorhombic structure has been analyzed with twinned[8] and detwinned[10] crystals. The anisotropy splits the zone-center mode by about 6 meV and the zone-edge mode by about 2 meV, and the overall dispersion is not strongly

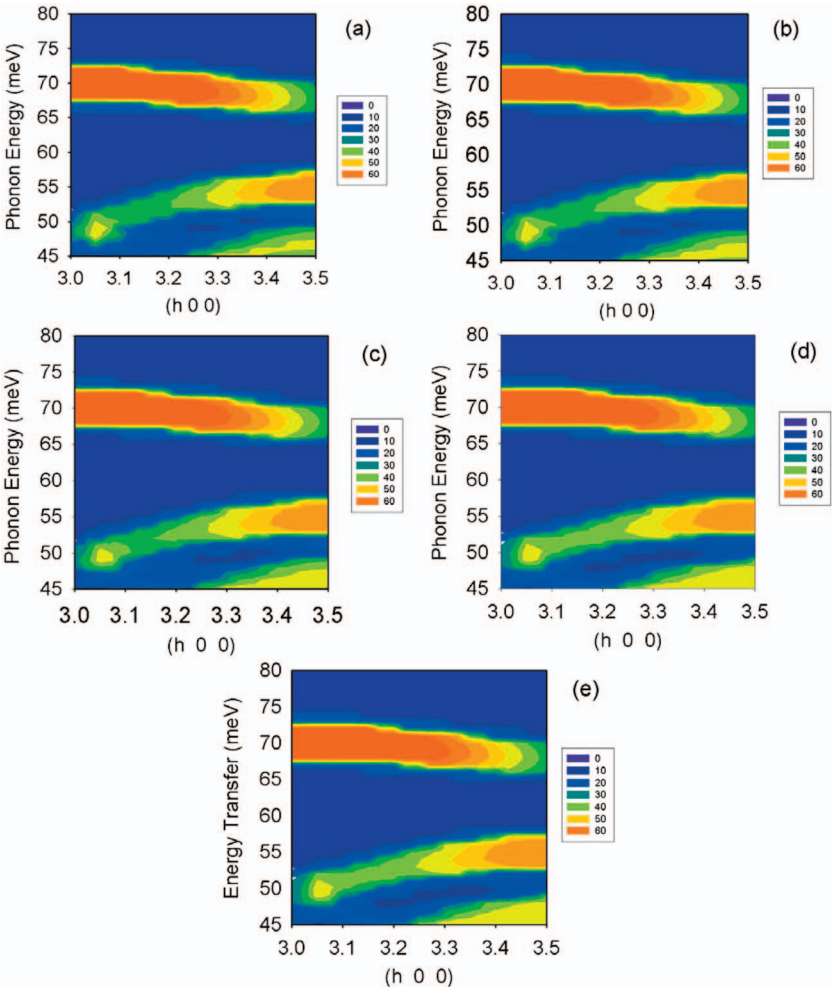

FIG. 5. (Color) (Series 1) Phonon intensities calculated with the shell model for (a) $YBa_2Cu_3O_{6.15}$, (b) $YBa_2Cu_3O_{6.35}$, (c) $YBa_2Cu_3O_{6.6}$, (d) $YBa_2Cu_3O_{6.7}$, and (e) $YBa_2Cu_3O_{6.95}$ from $\boldsymbol{Q}=(3,0,0)$ to (3.5, 0, 0). The shell model parameters were taken from Ref. 22. The parameters of interaction potentials were kept constant for all compositions, but charge density on the Cu-O plane was varied according to the nominal doping level of each compound. The model assumes an electronically homogeneous Cu-O plane.

affected. Thus, it is difficult to accept the proposed anisotropy for $YBa_2Cu_3O_{6.6}$,[9] which amounts to 12 meV at the middle of the zone. More importantly, as mentioned above, the same split into the high-energy and low-energy branches are seen even in $YBa_2Cu_3O_{6.35}$, which has no orthorhombic distortion. Thus, we conclude that the unusual dispersions for the samples with $x=0.35$, 0.6, and 0.7 cannot be explained in terms of the structural anisotropy.

The fact that two-phonon branches, high- and low-energy branches, are seen for the tetragonal $x=0.35$ sample is the most compelling reason that we have to consider inhomogeneity in charge distribution. It appears that the underdoped samples are made of two coexisting phases, one with a less hole density and with the phonon dispersion similar to that of

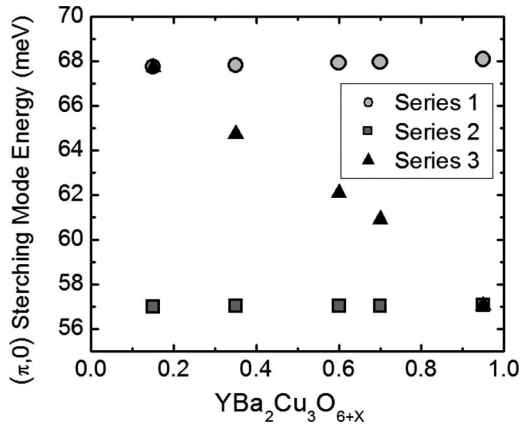

FIG. 6. The energy of the Cu-O bond-stretching mode at the zone edge, $(\pi,0)$. One of the models (Series 2) reproduced the experimentally observed energy reasonably well; the other two did not.

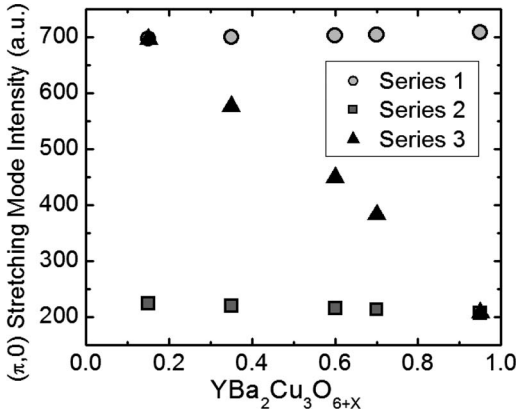

FIG. 7. Intensity of the bond-stretching mode at $(\pi,0)$. None of the models were able to reproduce the experimentally observed composition dependence of the intensity.

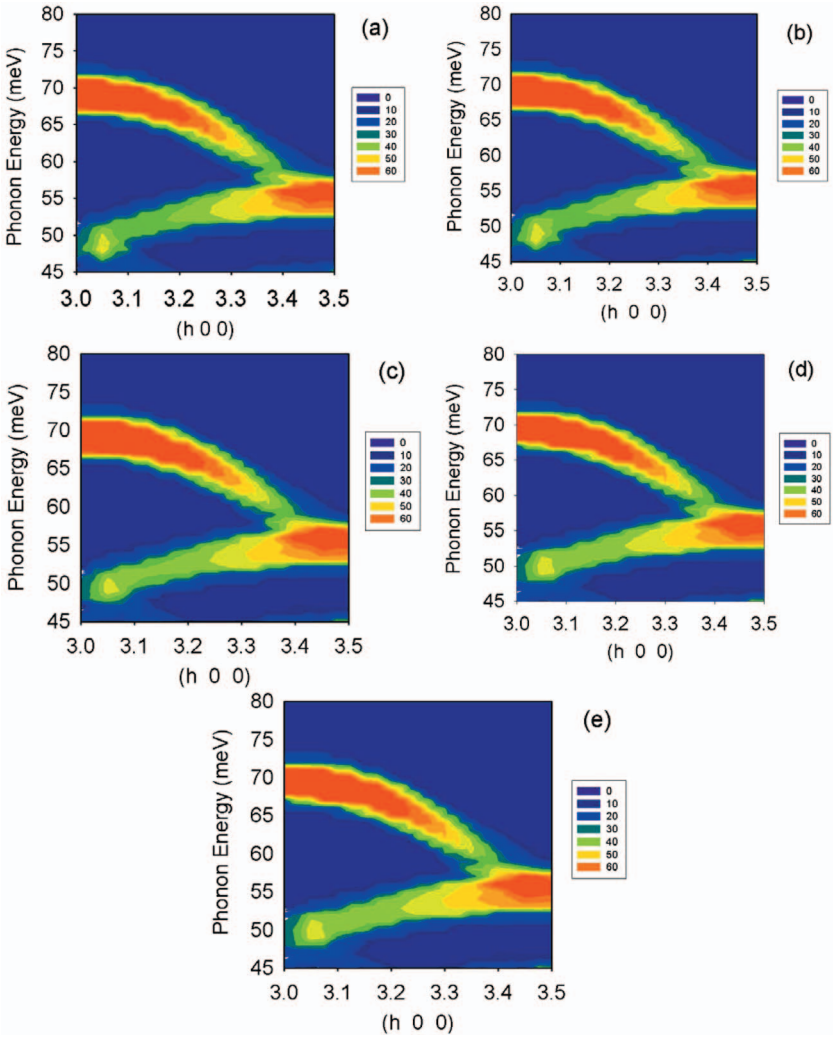

FIG. 8. (Color) (Series 2) The same as Fig. 5, but, in addition, harmonic potentials were introduced for Cu_{plane}-O_{plane}, Cu_{plane}-O_{apical}, and O_{plane}-O_{apical} to reproduce the zone-boundary softening of the in-plane Cu-O bond-stretching mode. The parameters of these potentials were kept constant for all compositions.

the undoped parent compound (type U), and the other with a higher hole density and with the dispersion similar to that of the optimally doped compound (type D). Increasing the average hole density increases the fraction of the type-D regions at the expense of the type-U regions, hence the spectral weight at the low-energy branch of the zone-boundary stretching mode. Here, as we will discuss below, we do not necessarily imply the hole density of the type-U region is zero and that of the type-D region is equal to the optimum hole density. However, we assume that some charge imbalance exists, and because of it the size of these regions has to be in the nanometer scale. It is not possible to make a reliable estimate of the size of the regions from the phonon dispersion since the high-energy portion of the phonon branch is nearly dispersionless, and the width of the low-energy branch is considerably wide.[1]

IV. DISCUSSION

The analysis of the results given above suggests that the observed phonon dispersion is most naturally explained by the nanoscale charge inhomogeneity in the underdoped cuprates. Actually, such charge inhomogeneity has long been suspected for the underdoped cuprates. Underdoped cuprates appear to consist of superconducting and nonsuperconducting regions. The volume fraction of the superconducting regions increases with doping, judged from the specific heat,[23] ARPES,[24] and the crystal field excitations measured by neutron scattering.[25] Nuclear quadrupole resonance (NQR) results for $La_{2-x}Sr_xCuO_4$ show a multiline structure for the in-plane Cu NQR spectrum, showing that the in-plane Cu has two distinct environments in $La_{2-x}Sr_xCuO_4$, with the density of one being proportional to x.[26] While it is possible that this type of Cu site corresponds to a Cu site next to a Sr dopant, the NQR on $La_2CuO_{4+\delta}$ shows an identical NQR spectrum for Cu,[27] even though in this case dopants are not positive Sr ions but negatively charged oxygen interstitials. It means that the Cu NQR effect has to originate from nearby localized holes and not by the impurity dopant.

The local atomic structure probed by extended x-ray-absorption fine structure also shows the presence of two different environments for Cu.[28,29] The observation of the spin-charge stripe state[30,31] indicates the propensity for charge separation in the cuprates. Scanning tunneling microscopy–scanning tunneling spectroscopy (STS) results indicate significant electronic inhomogeneity in BSCCO.[32–34] The distribution of the gap in the STS has a single broad peak rather than two peaks,[32,33] which may be because the STS detects mainly the pseudogap, rather than the superconducting gap.[35]

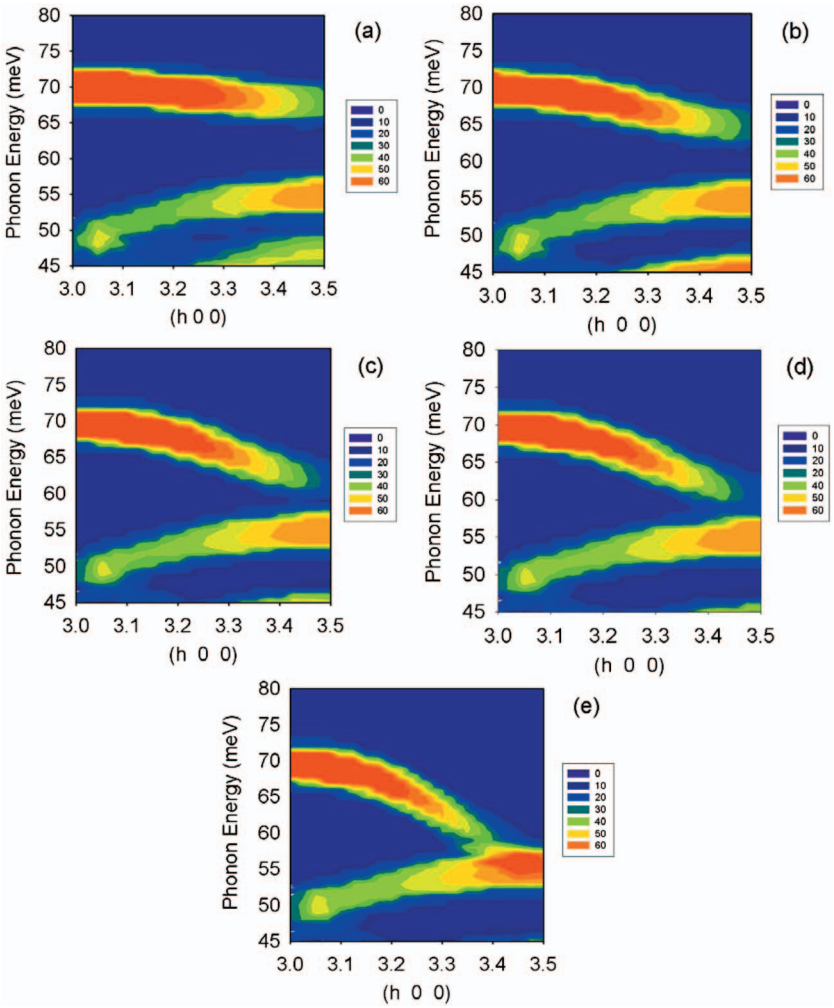

FIG. 9. (Color) (Series 3) Phonon intensities calculated as in Fig. 8. However, in addition to charge density in the CuO_2 plane, the strength of the harmonic potential (described earlier) was also varied. The first plot from the left shows phonon intensities when no harmonic terms are added; the following plots show intensities when the harmonic terms are gradually increased, proportionally to the charge density. The zone-boundary frequency of the Cu-O bond-stretching gradually decreases, contrary to the experimental observations.

The wide distribution in the gap size, however, is still consistent with strong electronic inhomogeneity.

The theoretical possibility of nanoscale electronic phase separation in the cuprates has been suggested by many.[36–39]

TABLE I. The coefficients and range (d) of the harmonic potential term $(1/2)k(r-r_0)^2$ introduced in the lattice dynamical model for noninsulating $YBa_2Cu_3O_{6+x}$ to reproduce the zone-boundary softening of the in-plane Cu-O bond-stretching mode.

	Pair	k (eV Å^{-2})	r_0 (Å)	d (Å)
$YBa_2Cu_3O_{6.35}$	O_{plane}-O_{plane}	−1.75	3.8872	4.0
	O_{plane}-O_{apical}	−1.6205	3.1923	3.3
	Cu_{plane}-O_{apical}	1.05	2.2917	2.4
$YBa_2Cu_3O_{6.6}$	O_{plane}-O_{plane}	−3.0	3.8872	4.0
	O_{plane}-O_{apical}	−2.778	3.1923	3.3
	Cu_{plane}-O_{apical}	1.8	2.2917	2.4
$YBa_2Cu_3O_{6.7}$	O_{plane}-O_{plane}	−3.5	3.8872	4.0
	O_{plane}-O_{apical}	−3.241	3.1923	3.3
	Cu_{plane}-O_{apical}	2.1	2.2917	2.4
$YBa_2Cu_3O_{6.95}$	O_{plane}-O_{plane}	−5.0	3.8872	4.0
	O_{plane}-O_{apical}	−4.63	3.1923	3.3
	Cu_{plane}-O_{apical}	3.0	2.2917	2.4

First-order phase transitions are always accompanied by the space in the phase diagram for a two-phase coexistence. Even in the case of the second-order transition, the negative curvature of the free energy as a function of composition leads to a possibility of phase separation. If there is sufficient ionic mobility, the system phase separates into two macroscopic electrically neutral phases with different doping levels, as in the case of $La_2CuO_{4+\delta}$.[40] However, at low temperatures where ionic mobility is absent, only electrons move, and two electrically charged phases with different doping levels are created. In this case, the Coulomb interaction prevents the phases from growing into a macroscopic size, and the phases remain in the nanoscale in dimension. A recent realistic estimate for the cuprates suggests that the cuprates either show such electronic phase separation or are on the verge of it.[41] Because of the long-range Coulomb interaction, the two phases could furthermore self-organize into an intermediate phase with a short-range order.[19] In most cases, the two phases do not represent the undoped and fully doped states. The actual difference in charge density between the two regions can be of the order of 0.1 or less, but could be sufficient to produce a significant difference in the degree of phonon softening near the zone edge. In addition, one of the phases could have static spins, for instance, with the short-range antiferromagnetic order or being in the spin-glass state. It has been suggested that the charge transfer between oxy-

gen and copper atoms is significantly suppressed by the local magnetic filed.[42] Thus, the presence of static spins will suppress the softening of the bond-stretching mode and could lead to the observed two-state behavior of the phonon dispersion in $YBa_2Cu_3O_{6+x}$. At this moment, it is not clear if similar nanoscale phase separation exists or not for other cuprates, such as $La_{2-x}Sr_xCuO_4$. While Ref. 6 shows similar splitting of the branches for $La_{1.85}Sr_{0.15}CuO_4$ at low temperatures, suggesting nanoscale phase separation, Refs. 12 and 13 appear to show no splitting.

V. CONCLUSIONS

Inelastic neutron scattering studies carried out on crystals of the superconducting cuprates revealed strong dependence of the energy of the Cu-O bond-stretching LO phonon mode on the doped hole density. In this work, we carried out a more detailed study on $YBa_2Cu_3O_{6+x}$, focusing not only on the dispersion, but also on the spectral intensity, of the Cu-O bond-stretching LO phonon mode as they vary with the hole density. The results are best explained in terms of the microscopic two-state model, with and without softening, and are consistent with the nanoscale electronic phase separation in the underdoped $YBa_2Cu_3O_{6+x}$. This work adds to the long list of literature that theoretically or experimentally suggests nanoscale electronic phase separation in the superconducting cuprates. The relevance of such electronic phase separation to the microscopic mechanism of high-temperature superconductivity, however, is still controversial.

ACKNOWLEDGMENTS

The authors are grateful to K. A. Müller, L. P. Gor'kov, A. Bussmann-Holder, D. Reznik, E. Dagotto, and A. Moreo for useful discussions. The work carried out at the University of Pennsylvania and at the University of Tennessee was supported by the National Science Foundation through DMR04-04781.

[1] L. Pintschovius and W. Reichardt, in *Physical Properties of High Temperature Superconductors IV*, edited by D. Ginsberg (World Scientific, Singapore, 1994), p. 295.
[2] S. L. Chaplot, W. Reichardt, L. Pintschovius, and N. Pyka, Phys. Rev. B **52**, 7230 (1995).
[3] C. Falter, M. Klenner, G. A. Hoffmann, and Q. Chen, Phys. Rev. B **55**, 3308 (1997).
[4] G. Khaliullin and P. Horsch, Physica C **282-287**, 1751 (1997).
[5] O. Rösch and O. Gunnarsson, Phys. Rev. Lett. **92**, 146403 (2004).
[6] R. J. McQueeney, Y. Petrov, T. Egami, M. Yethiraj, G. Shirane, and Y. Endoh, Phys. Rev. Lett. **82**, 628 (1999).
[7] D. Reznik, L. Pintschovius, M. Ito, S. Ikubo, M. Sato, H. Goka, M. Fujita, K. Yamada, G. D. Gu, and J. M. Tranquada, Nature (London) **440**, 1170 (2006).
[8] J.-H. Chung, T. Egami, R. J. McQueeney, M. Yethiraj, M. Arai, T. Yokoo, Y. Petrov, H. A. Mook, Y. Endoh, S. Tajima, C. Frost, and F. Dogan, Phys. Rev. B **67**, 014517 (2003).
[9] L. Pintschovius, W. Reichardt, M. Kläser, T. Wolf, and H. v. Löhneysen, Phys. Rev. Lett. **89**, 037001 (2002).
[10] L. Pintschovius, D. Reznik, W. Reichardt, Y. Endoh, H. Hiraka, J. M. Tranquada, H. Uchiyama, T. Masui, and S. Tajima, Phys. Rev. B **69**, 214506 (2004).
[11] R. J. McQueeney, J. L. Sarrao, P. G. Pagliuso, P. W. Stephens, and R. Osborn, Phys. Rev. Lett. **87**, 077001 (2001).
[12] T. Fukuda, J. Mizuki, K. Ikeuchi, K. Yamada, A. Q. R. Baron, and S. Tsutsui, Phys. Rev. B **71**, 060501(R) (2005).
[13] L. Pintschovius, D. Reznik, and K. Yamada, Phys. Rev. B **74**, 174514 (2006).
[14] S. Ishihara, T. Egami, and M. Tachiki, Phys. Rev. B **55**, 3163 (1997).
[15] Y. Petrov and T. Egami, Phys. Rev. B **58**, 9485 (1998).
[16] P. Piekarz and T. Egami Phys. Rev. B **72**, 054530 (2005).
[17] A. Lanzara, P. V. Bogdanov, X. J. Zhou, S. A. Keller, D. L. Feng E. D. Lu, T. Yoshida, H. Eisaki, A. Fujimori, K. Kishio, J.-I. Shimoyama, T. Noda, S. Uchida, Z. Hussain, and Z.-X. Shen, Nature (London) **412**, 510 (2001).
[18] G.-H. Gweon, T. Sasagawa, S. Y. Zhou, J. Graf, H. Takagi, D. H. Lee, and A. Lanzara, Nature (London) **430**, 187 (2004).
[19] T. Egami, in *High T_C Superconductors and Related Transition Metal Oxides: Special Contributions in Honor of K. Alex Müller and the Occasion of His 80th Birthday*, edited by A. Bussmann-Holder and H. Keller (Springer-Verlag, Berlin, 2007), p. 103.
[20] J.-H. Chung, Ph.D. thesis, University of Pennsylvania, 2003.
[21] T. Egami, AIP Conf. Proc. **535**, 16 (2000).
[22] W. Kress, U. Schröder, J. Prade, A. D. Kulkarni, and F. W. de Wette, Phys. Rev. B **38**, 2906 (1988).
[23] J. W. Loram, J. Luo, J. R. Cooper, W. Y. Liang, and J. L. Tallon, J. Phys. Chem. Solids **62**, 59 (2001).
[24] D. L. Feng, D. H. Lu, K. M. Shen, C. Kim, H. Eisaki, A. Damascelli, R. Yoshizaki, J.-i. Shimoyama, K. Kishio, G. D. Gu, S. Oh, A. Andrus, J. O'Donnell, J. N. Eckstein, and Z.-X. Shen, Science **289**, 277 (2000).
[25] J. Mesot, P. Allenspach, U. Staub, A. Furrer, H. Mutka, R. Osborn, and A. Taylor, Phys. Rev. B **47**, 6027 (1993).
[26] Y.-Q. Song, M. A. Kennard, M. Lee, K. R. Poeppelmeier, and W. P. Halperin, Phys. Rev. B **44**, 7159 (1991).
[27] P. C. Hammel, A. P. Reyes, S.-W. Cheong, Z. Fisk, and J. E. Schirber, Phys. Rev. Lett. **71**, 440 (1993).
[28] A. Bianconi, N. L. Saini, A. Lanzara, M. Missori, T. Rossetti, H. Oyanagi, H. Yamaguchi, K. Oka, and T. Ito, Phys. Rev. Lett. **76**, 3412 (1996).
[29] N. L. Saini, H. Oyanagi, T. Itoh, V. Scagnoli, M. Filippi, S. Agrestini, G. Campi, K. Oka, and A. Bianconi, Eur. Phys. J. B **36**, 75 (2003).
[30] J. M. Tranquada, H. Woo, T. G. Perring, H. Goka, G. D. Gu, G. Xu, M. Fujita, and K. Yamada, Nature (London) **429**, 534 (2004).
[31] P. Abbamonte, A. Rusydi, S. Smadici, G. D. Gu, G. A. Sawatzky, and D. L. Feng, Nat. Phys. **1**, 155 (2005).
[32] S. H. Pan, J. P. O'Neal, R. L. Badzey, C. Chamon, H. Ding, J. R. Engelbrecht, Z. Wang, H. Eisaki, S. Uchida, A. K. Gupta, K.-W.

Ng, E. W. Hudson, K. M. Lang, and J. C. Davis, Nature (London) **413**, 282 (2001).
[33] K. M. Lang, V. Madhavan, J. E. Hoffman, E. W. Hudson, H. Eisaki, S. Uchida, and J. C. Davis, Nature (London) **415**, 412 (2002).
[34] Y. Kohsaka, C. Taylor, K. Fujita, A. Schmidt, C. Lupien, T. Hanaguri, M. Azuma, M. Takano, H. Eisaki, H. Takagi, S. Uchida, and J. C. Davis, Science **315**, 1380 (2007).
[35] G. Deutscher, Nature (London) **397**, 410 (1999).
[36] L. P. Gor'kov and A. V. Sokol, JETP Lett. **46**, 420 (1987).
[37] V. J. Emery, S. A. Kivelson, and H. Q. Lin, Phys. Rev. Lett. **64**, 475 (1990).
[38] E. Dagotto, Rev. Mod. Phys. **66**, 763 (1994).
[39] S. A. Kivelson, Nat. Mater. **5**, 343 (2006).
[40] P. G. Radaelli, J. D. Jorgensen, R. Kleb, B. A. Hunter, F. C. Chou, and D. C. Johnston, Phys. Rev. B **49**, 6239 (1994).
[41] B. Fine and T. Egami, arXiv:0707.3994, Phys. Rev. B (to be published).
[42] P. Piekarz (unpublished).